



**Repositorio Institucional de la Universidad Autónoma de Madrid**

<https://repositorio.uam.es>

Esta es la **versión de autor** del artículo publicado en:

This is an **author produced version** of a paper published in:

Chemical Engineering Journal 348 (2018): 661-668

**DOI:** <http://doi.org/10.1016/j.cej.2018.05.029>

**Copyright:** © 2018 Elsevier B.V.

El acceso a la versión del editor puede requerir la suscripción del recurso

Access to the published version may require subscription

# **From Kinetics to Equilibrium Control in CO<sub>2</sub> capture columns using Encapsulated Ionic Liquids (ENILs)**

R. Santiago, J. Lemus, D. Moreno, C. Moya, M. Larriba, N. Alonso-Morales, M.A.

Gilarranz, J.J. Rodríguez and J. Palomar\*

*Sección de Ingeniería Química. Universidad Autónoma de Madrid. 28049 Madrid. Spain.*

\*Corresponding author. E-mail: pepe.palomar@uam.es

Keywords: CO<sub>2</sub> capture; Ionic Liquids; ENIL; Physical Absorption; ILUAM; Aspen

## **Abstract**

A novel approach based on Encapsulated Ionic Liquids (ENILs) is proposed for overcoming the mass transfer constraints in CO<sub>2</sub> physical absorption by ILs. Absorption process simulation using COSMO-based/Aspen Plus methodology -an a priori approach- was carried to select four ILs with high and similar CO<sub>2</sub> absorption capacity but markedly different transport properties: EmimTCM, BmimTCM, BmimDCN, and BmimOcSO<sub>4</sub>. Simulations using equilibrium- and rate-based column models for these ILs showed that CO<sub>2</sub> recovery and the absorbent performance are severely reduced when the viscosity of the IL increases. Experimental gravimetric analyses with the selected ILs confirmed the large differences in solubility and absorption rate, this last also dependent on viscosity. ENILs were prepared by encapsulation of ILs in hollow carbon sub-microcapsules with a porous shell. The experimental gravimetric analysis evidenced that the ILs maintain their CO<sub>2</sub> absorption capacity after encapsulation, whereas the absorption rate is ca. 50 times higher for ENILs than neat ILs. ENIL tests in fixed bed operation at different operating conditions yielded bed utilization values dependent on the CO<sub>2</sub> solubility in the

ENIL, while equivalent mass transfer zone lengths were obtained for all the materials. The results demonstrate the fast CO<sub>2</sub> mass transfer rates in ENILs -related to the high contact area provided- allows overcoming the mass transfer limitations controlling the CO<sub>2</sub> rate of physical absorption by ILs.

## **Introduction**

The greenhouse effect and global warming caused by CO<sub>2</sub> have become serious environmental concerns and have awakened the population attention <sup>[1]</sup>. One of the most promising methodologies for limiting the global warming effects caused by greenhouse gases consists on the direct physical or chemical absorption of CO<sub>2</sub> from post-combustion streams due to their efficiency and lower cost <sup>[2] [3]</sup>. Regarding physical absorption, solvents such as Purisol <sup>[4]</sup>, Rectisol <sup>[5]</sup> and Selexol <sup>[6]</sup>, among others, are used to capture CO<sub>2</sub> working at high pressure. However, they present problems such as corrosive nature, toxicity and high volatility resulting in high solvent losses <sup>[3]</sup>. On the other hand, amines <sup>[7]</sup> are widely used in chemical absorption processes<sup>[8]</sup>, but they present degradation and corrosivity, resulting in high solvent losses, environmental impact and substantial maintenance costs <sup>[9]</sup>.

Therefore, there is a demand for innovative and cost-effective technologies capable of efficiently capturing CO<sub>2</sub>, overcoming these problems of commercially available systems. In this sense, ILs are presented as promising novel solvents, which have attracted growing interests as shown by the number of studies on CO<sub>2</sub> capture <sup>[10]</sup>. The advantages of using ILs as absorbents are their high and tailorable absorption capacity, low vapor pressure and high thermal stability. However, they present some disadvantages such as: high price, environmental-concerns and limitations in their transport properties. The high viscosity of ILs is probably the main technical limitation for their practical application

<sup>[11]</sup>, which can even increase in some cases due to the dissolution of CO<sub>2</sub> <sup>[12]</sup>. In fact, recent process simulation analyses have demonstrated that the efficiency of CO<sub>2</sub> capture by physical absorption in packed columns is severely reduced by the strong kinetic control of the operation, obtaining CO<sub>2</sub> recoveries significantly lower than those expected from the high absorption capacities of ILs <sup>[13]</sup>. Therefore, modifications of neat ILs may be necessary before they can be widely accepted for CO<sub>2</sub> separation <sup>[14]</sup>.

The Encapsulated Ionic Liquid (ENIL) concept has been proposed as a promising alternative to overcome the mass transfer rate limitations of separation process based on ILs <sup>[15]</sup>. ENILs consist of hollow carbonaceous sub-microcapsules (C<sub>cap</sub>) filled with ILs <sup>[16]</sup>. The synthesis of ENILs is favored by the high affinity between ILs and porous carbons <sup>[17]</sup>. The ENILs can be prepared with a high proportion of IL (75-85 % in weight) and small capsule size (500-700 nm). Therefore, the ENIL material involves a change from continuous to discrete IL phase with submicrometric drop size. Due to ENIL morphology, the specific contact area is drastically increased with respect to the neat IL, enhancing the rate of mass transfer phenomena but maintaining the properties of the ILs as solvents <sup>[15]</sup>. This novel approach, based on ENIL materials has been successfully applied to NH<sub>3</sub> separation <sup>[18]</sup> and CO<sub>2</sub> capture based on chemical absorbents as acetate-based ILs.<sup>[19]</sup> Recently, ENIL systems were also efficiently applied in CO<sub>2</sub> capture by physical absorption with ILs <sup>[20]</sup>. From an economical point of view, ENIL materials would not only improved the mass transport properties, but also enhance the regeneration step and take advantage from the amount of IL used, becoming a more effective material than neat LIs.

On the other hand, the evaluation of IL performance in practical applications at industrial scale is a key issue in the development of new separation processes based on ILs <sup>[21]</sup>. In the last years, our group has developed the COSMO-based/Aspen Plus multiscale

methodology - based on integrating molecular and process simulation tools- of great utility in the preliminary: i) selection of ILs attending to thermodynamic, kinetic, technical or economical criteria; and ii) viability analysis of the proposed IL-based process and comparison to available technologies <sup>[22]</sup>. COSMO-based/Aspen methodology has been tested in the study of IL regeneration by distillation <sup>[23]</sup> and in toluene <sup>[24]</sup> and acetylene <sup>[25]</sup> absorption. In addition, it was applied to aromatic-aliphatic separation by liquid-liquid extraction <sup>[26]</sup> or by extractive distillation <sup>[27]</sup>, CO<sub>2</sub> capture by physical absorption <sup>[13]</sup> and absorption refrigeration cycles based on ILs <sup>[28]</sup>. Since COSMO-based/Aspen methodology is an *a priori* approach, which does not require experimentation, process simulations can also be an alternative or a previous step to the experimentation, with the aim of reducing and focusing the number of ILs studied and, thereby, minimizing the consumption of resources in experimental work-.

The objective of this work is to evaluate the potential application of ENIL materials in the capture of CO<sub>2</sub> by physical absorption with ILs. For this purpose, unfavorable conditions from the kinetic point of view were selected, i.e. postcombustion processes (10-13% CO<sub>2</sub> concentrations). Firstly, process simulations using COSMO-based/Aspen Plus methodology are carried out to evaluate the behavior of a large set of ILs in the physical absorption of CO<sub>2</sub> in commercial packed columns. From this theoretical analysis, a selection of 4 ILs with similar absorption capacities (provided by equilibrium-based column model) and markedly different kinetic behavior (provided by the Rated-Based column model) is made. The reason to select ILs providing different absorption rates is to analyze if the encapsulation in ENILs maintain the CO<sub>2</sub> absorption capacity of ILs and also improves the kinetics of the CO<sub>2</sub> uptake. The ILs selected were characterized using a high-pressure microbalance to obtain CO<sub>2</sub> absorption capacities and CO<sub>2</sub> diffusion values at three temperatures and pressures (301-333 K and 1-6 bar). The next

step is the synthesis and characterization of ENIL materials using the previously selected ILs. The ENIL were tested in gravimetric essays to analyze their CO<sub>2</sub> sorption capacity and rate. Finally, fixed-bed sorption experiments were carried out at temperatures from 303 to 333 K and 0.1 bar CO<sub>2</sub>, in order to evaluate if the application of the proposed approach based on ENIL systems allows overcoming the mass transfer rate limitations of the CO<sub>2</sub> physical absorption by the free ILs.

## **Experimental section**

### **Materials**

The ILs 1-butyl-3-methylimidazolium dicyanamide (95 %) BmimDCN, 1-butyl-3-methylimidazolium tricyanomethanide (95 %) BmimTCM and 1-ethyl-3-methylimidazolium tricyanomethanide (95 %) EmimTCM were purchased from Iolitec and 1-butyl-3-methylimidazolium octylsulfate (95 %) BmimOcSO<sub>4</sub> from Sigma-Aldrich. The synthesis of the hollow sub-microcapsules was carried out using phenol (99 %), paraformaldehyde (95-100 %), aluminum trichloride (95-100 %), ammonia (34 %) and absolute ethanol supplied by Panreac. Tetraethylorthosilicate (98 %) (TEOS), hexadecyltrimethoxysilane (90 %) (C16TMS) and hydrofluoric acid (48 %) were supplied by Sigma-Aldrich. Carbon dioxide, nitrogen, and helium were supplied by Praxair, Inc., with a minimum purity of 99.999 %. Furthermore, a mixture containing 10,000 ppmv of carbon dioxide in nitrogen was supplied by Praxair, Inc and used in fixed bed capture experiments.

Before the absorption experiments, all the ILs and ENIL materials used were dried and degassed at 333 K under vacuum ( $10^{-3}$  mbar) during 24 h to ensure a water content lower than 200 ppm.

## **ENIL preparation and characterization**

The hollow sub-microcapsules ( $C_{\text{Cap}}$ ) synthesized for their use as ENIL support were prepared following the methodology reported by our group in previous works <sup>[16, 18-19]</sup> and based on the procedure described by Büchel et al <sup>[29]</sup>. In summary,  $C_{\text{Cap}}$  were prepared by a templating method using an aluminosilicate template formed by a solid core and a mesoporous shell. A phenolic resin was infiltrated into the template to serve as a carbon precursor. Then, the infiltrated template was subjected to pyrolysis at 700°C during 5 hours and the template was removed using HF.

The ENIL materials were prepared by incipient wetness impregnation of 100 mg of  $C_{\text{Cap}}$  with 1 mL of an IL-acetone solution. The solution was added dropwise onto the support. After impregnation acetone was removed by evaporation at 333 K during 24 h. In the current work, the four ENIL tested were prepared with an IL nominal load of 80 %w/w. The amount of IL incorporated was checked by elemental analysis. This methodology was successfully applied in our previous publications allowing a homogeneous distribution of the IL inside the  $C_{\text{Cap}}$  <sup>[18-19]</sup>.

The CHN content of the hollow sub-microcapsules and ENIL materials were characterized by elemental analysis in a LECO CHNS-932 apparatus. The IL amount loaded into the spheres could be calculated by this characterization essay". Then, the porous texture of the carbon material was characterized by 77 K  $N_2$  adsorption/desorption in a TriStar II 3020 (Micromeritics) system after 12 h of degassing at 0.1 mbar and 393 K. The surface area was calculated by using the BET equation. The microstructure and morphology of  $C_{\text{Cap}}$  and ENILs were studied by scanning electron microscopy (SEM) and transmission electron microscopy (TEM). SEM analyses were performed with a Hitachi

S-3000N apparatus and TEM images were obtained in Philips 420, JEM-2000 FX and JEM-4000 EX microscopes.

### **Gravimetric CO<sub>2</sub> absorption measurements**

The measurements of CO<sub>2</sub> solubility (mg CO<sub>2</sub> /g IL) in ILs and ENILs were performed in a gravimetric high-pressure sorption analyzer (ISOSORP GAS LP-flow, Rubotherm) equipped with a magnetic suspension balance (MSB). The balance covers a weight range up to 10 g, with a precision of 10<sup>-5</sup> g. In addition, it can operate in a wide range of temperatures (from room temperature to 150 °C) and pressures (from 10<sup>-3</sup> mbar to 30 bar). A full description of the thermogravimetric experimental methodology is available in previous works <sup>[30]</sup>.

The CO<sub>2</sub> absorption isotherms for the four selected ILs and their corresponding ENILs were obtained at three different temperatures (301.5, 316.5 and 331.5 K) and three different pressures (1, 3 and 6 bar). In a standard run a 100 mL/min flow of pure CO<sub>2</sub> at 1 bar is passed through the sorbent sample (100-150 mg for neat IL and ENIL materials) and the increase in the mass is recorded over the time at fixed temperature. Once the sample is saturated, i.e. weight change < 0.02 mg/h, the pressure is increased. The buoyancy effect is corrected and the amount of CO<sub>2</sub> absorbed is quantified in terms of as mg of CO<sub>2</sub> per g of IL and molar ratio ( $z_{CO_2}$ ):

$$z_{CO_2} = \frac{m_{CO_2}/M_{CO_2}}{m_{IL}/M_{IL}} \quad (1)$$

Where  $m_{CO_2}$  is the absorbed CO<sub>2</sub> mass,  $m_{IL}$  is the IL mass after degasification and  $M_{CO_2}$  and  $M_{IL}$  are the molecular weights of CO<sub>2</sub> and IL, respectively.



The CO<sub>2</sub> diffusion coefficients in the different ILs were estimated from gravimetric analysis by using a mass diffusion model reported by Shifflet and Yokozeki <sup>[31]</sup> and later used by other authors <sup>[30]</sup> for CO<sub>2</sub>-IL systems. The proposed model assumes linear diffusion of the CO<sub>2</sub> over a quiescent mass of IL placed in the bottom of a sample container <sup>[31]</sup>. In these conditions the CO<sub>2</sub> diffusion can be expressed as follows:

$$\frac{\partial C}{\partial t} = D \cdot \frac{\partial^2 C}{\partial z^2} \quad (2)$$

Where  $C$  is the concentration of CO<sub>2</sub> in the IL at a given time ( $t$ ) and  $D$  is the diffusion coefficient of CO<sub>2</sub> in the IL. Initial conditions consider that  $C = C_0$  when  $t = 0$  and  $0 < z < L$ , and boundary conditions are: i)  $C = C_s$  when  $t > 0$  and  $z = 0$ ; ii)  $\partial C / \partial z = 0$  at  $z = L$ , where  $z$  is a vertical location and  $L$  is the depth of IL in the container, which is calculated by using the volume of the sample and the inner diameter of the container (1.5 cm). The integration of Eq. 2 leads to:

$$\bar{C} = C_s \cdot \left[ 1 - 2 \cdot \left( 1 - \frac{C_0}{C_s} \right) \cdot \sum_{n=0}^{\infty} \frac{\exp(-\lambda_n^2 \cdot D \cdot t)}{L^2 \cdot \lambda_n^2} \right] \quad (3)$$

Where  $C_0$  and  $C_s$  are respectively the CO<sub>2</sub> initial and saturation concentration at each temperature and pressure,  $\bar{C}$  is the CO<sub>2</sub> concentration at each time,  $D$  is the diffusivity,  $t$  is the time,  $L$  is the height of the sample (calculated from the sample density and mass and almost 2.2 mm in all cases) and  $\lambda_n$  a parameter calculated from Eq. 4:

$$\lambda_n = \left( n + \frac{1}{2} \right) \cdot \frac{\pi}{L} \quad (4)$$

Finally, the time-dependent data obtained from the gravimetric measurements were fitted to Eq. 3 to obtain the diffusion coefficient. Although Eq. 3 shows a sum of infinite terms, only the first ten terms are enough for the calculation in practical applications.

### Fixed-bed CO<sub>2</sub> sorption experiments

The fixed-bed experiments were carried out in a Microactivity unit (PID Eng&Tech, Spain) provided with a stainless-steel tube of 9.5 mm of internal diameter and 15 cm of length and a distributor of sintered stainless-steel. The tube is placed into a furnace which allows controlling the temperature from almost ambient to 573 K. The pressure inside the fixed bed can be controlled from atmospheric to 20 bar. The outlet gas flow was analyzed by an Agilent 7820A gas chromatograph equipped with a 20 m column (Agilent PoraPlot U) and a TCD detector, which allows calculating the CO<sub>2</sub> concentration. For each experiment, the fixed bed was loaded with 4 g of fresh ENIL, i.e. a bed height ( $H$ ) of ~15 cm. The inlet gas is continuously fed through the fixed bed composed of an N<sub>2</sub>-CO<sub>2</sub> mixture (10 % v/v of CO<sub>2</sub>) with a flow of 3.3 NmL/min. For each ENIL, breakthrough curves at three different temperatures (303, 318 and 333 K) at 1 bar of total pressure were obtained. Once the ENIL material was saturated, the furnace temperature was increased to 333 K for regenerating it. We did not appreciate any capacity difference before and after the regeneration step which allows us using the ENIL material in different sorption-desorption cycles. A blank experiment was performed with the fixed bed loaded with inert material with the same bed height as ENILs. In that way, the calculations were done by subtracting the blank measurement curve at each temperature to the breakthrough curve of each ENIL material at that temperature. The sorption capacity ( $q_e$ , mg/g) was calculated from the breakthrough curves using the following equation:

$$q_e = \frac{Q}{m} \cdot \int_0^{t_s} (C_o - C) dt \quad (4)$$

where  $Q$  is the gas flow rate (L/min)),  $m$  is the ENIL mass (g) in the fixed bed,  $C$  and  $C_0$  are respectively the outlet and the inlet concentration (g/L), and  $t_s$  is the saturation time (min). The breakthrough curves were fitted to the equation described by Yoon and Nelson [32].

$$t = t_{0.5} + \frac{1}{k} \cdot \ln\left(\frac{C}{C_0 - C}\right) \quad (5)$$

Where  $t$  is the operation time (min),  $t_{0.5}$  is the time at which the outlet concentration is half of the inlet one (min), and  $k$  is the Yoon and Nelson constant ( $\text{min}^{-1}$ ), which is used in our study as kinetic key parameter for comparing the ENILs tested. This model has been successfully applied in sorption operations using fixed beds [32-33]. The length of the mass transfer zone ( $H_{MTZ}$ ) was calculated from each breakthrough curve as an additional parameter to evaluate the kinetics of the process using the equation:

$$H_{MTZ} = H \cdot \frac{(t_{0.95} - t_{0.05})}{t_{0.95}} \quad (6)$$

Where  $H$  is the height of the bed, and  $t_{0.05}$  and  $t_{0.95}$  are the time at which the outlet  $\text{CO}_2$  concentration reaches 5 % and 95 % of the inlet one, respectively. The bed utilization fraction ( $f$ ) was estimated from  $H_{MTZ}$ , considering an antisymmetric breakthrough curve:

$$f = 1 - \frac{0.5 H_{MTZ}}{H} \quad (7)$$

### Process simulation details

COSMO-based/Aspen Plus methodology was applied to model the  $\text{CO}_2$  physical absorption by IL in a column with a commercial packing using *Equilibrium-* and *Rate-based* models [13]. ILUAM database [22] was used to incorporate 44 ILs as pseudo-components in Aspen Plus v9.0 (they are not available as conventional compounds in the

extensive Aspen Properties database) to perform process simulation using COSMOSAC property package which only need theoretical information obtained from COSMO-RS software to define the ILs (molecular weight, density at 60 °F, boiling point,  $\sigma$ -profile and COSMO volume) and also includes experimental viscosity and its dependence with the temperature. For more details on this methodology, see the work developed by Ferro *et al.* [22]. The selection of 44 ILs for this study was done based on different commercial cations/anions combinations widely studied in the literature for CO<sub>2</sub> physical absorption. The CO<sub>2</sub> absorption operation using ILs was modeled using the *RADFRAC* column model implemented as default in Aspen Plus v9.0. The operating conditions were selected based on a CO<sub>2</sub> capture operation at pilot plant scale studied in previous works [13]. The gas feed was defined as a 1000 kmol/h (30 ton/h) stream with 13%v of CO<sub>2</sub> and 87%v of N<sub>2</sub> at 303 K and 1 atm of total pressure. The IL stream was defined as a pure IL stream with a flow rate of 400 ton/h (L/G = 13, weight). The *RADFRAC* column was specified as an absorption column without condenser or reboiler with 10 equilibrium stages. First, the equilibrium model, in which mass transfer kinetic is not taken into account, was used. Once the calculation in equilibrium mode was converged, the rate-based calculation was specified. In this stage, the definition of the type of internal packing used in the column is needed. As in previous works [13, 24], 0.625-in FLEXIRING KOCH Metal packing was used in this study. Column diameters were calculated to ensure a column capacity of 62  $\pm$  5%, and based on these results a column height of 20 m was chosen for assuring a height/diameter ratio of almost 10. The recovery of CO<sub>2</sub> was calculated as the ratio between the CO<sub>2</sub> absorbed by the IL and the CO<sub>2</sub> in the gas feed.

## Results

### Process simulation

Figure 1A compares the CO<sub>2</sub> recoveries achieved for 44 commercial ILs in a packed column at fixed operating conditions using *RADFRAC Equilibrium* mode (only thermodynamics is considered) and *Rate-based* mode (mass transfer kinetic is also taken into account) simulations. As can be seen, there is a wide range of recoveries for the studied ILs. When *Equilibrium* mode is analyzed, the ILs considered provide recoveries of CO<sub>2</sub> ranging from 46 % to 98 % at fixed operating conditions (see “Process simulation details” section). In contrast, when the absorption kinetics is taken into account in the calculations by using the *Rate-based* mode, drastic reductions in the CO<sub>2</sub> recovery are obtained at identical operating conditions, with values from 0.3 to 62 % for the more viscous ILs. From these results, it can be inferred that despite the very high CO<sub>2</sub> recoveries in *Equilibrium* mode obtained for the majority of the ILs, when the mass transfer kinetics is considered they can present very different behaviors. From these results, we have selected four ILs (EmimTCM, BmimTCM, BmimDCN and BmimOcSO<sub>4</sub>, red circles in Figure 1) that show similar absorption efficiency attending to the thermodynamics (almost 91% CO<sub>2</sub> recovery in *Equilibrium* mode), but show different recovery values in the range of kinetic behavior (from 1% to 62 % of CO<sub>2</sub> recovery in *Rate-based* mode). These ILs were selected for the experimental study and encapsulated in ENIL systems in next stages of this work. Figure 1B shows the CO<sub>2</sub> recoveries obtained using *Rate-based* simulations as a function of the viscosity of ILs at 303 K. As can be seen, the recovery of CO<sub>2</sub> decreases markedly when the viscosity of the IL increases,

regardless of their CO<sub>2</sub> absorption capacity. Negligible CO<sub>2</sub> recovery is obtained when IL viscosity is higher than 200 cP.

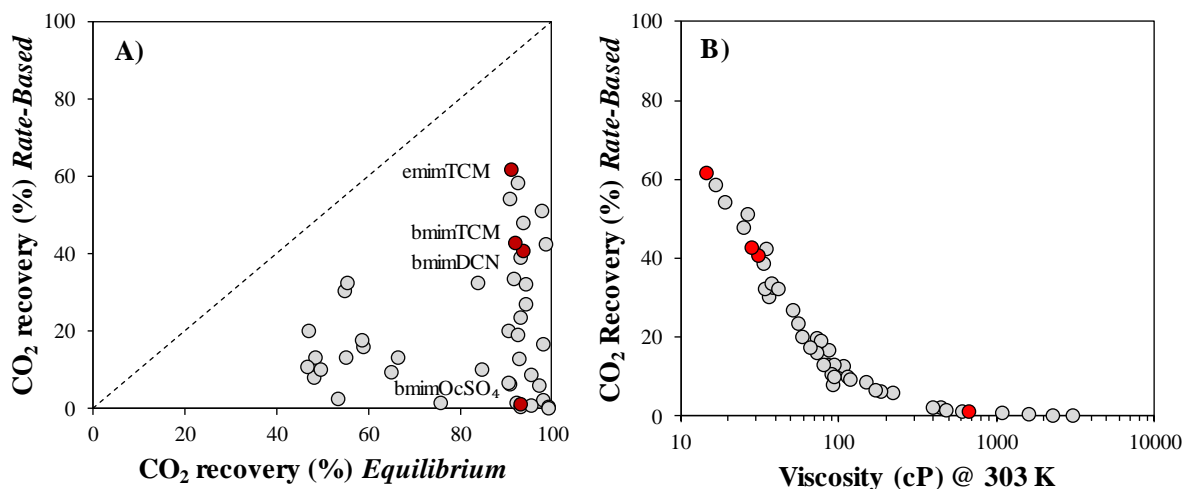


Figure 1: (A) CO<sub>2</sub> recoveries for 44 ILs calculated by Aspen Plus process simulator using *Rate-based* and *Equilibrium* modes of RADFRAC column; (B) CO<sub>2</sub> recoveries for 44 ILs calculated using Rate-based mode vs viscosity of ILs at 303 K. Red circles: ILs selected for the experimental study.

### Gravimetric CO<sub>2</sub> absorption by ILs

Thermodynamic and kinetic analyses of CO<sub>2</sub> physical absorption by the selected ILs (EmimTCM, BmimTCM, BmimDCN, and BmimOcSO<sub>4</sub>) were carried out by gravimetric measurements in the MSB equipment at three different pressures (1, 3 and 6 bar) and temperatures (301, 316 and 331 K). Table 1 shows the physical properties of the ILs selected. From the recorded increase of mass of the IL sample over the time, the CO<sub>2</sub> absorption capacity and CO<sub>2</sub> diffusion coefficient ( $D$ ) for each IL were estimated at the different operating conditions (Table 2). As can be seen, the four selected ILs present nearly the same CO<sub>2</sub> solubility values (from 3.1 to 3.8 mg·g<sup>-1</sup> at 1 bar and 301.5 K), *i. e.* they show similar solvent performance from a thermodynamic point of view. These results are in agreement with the conclusion achieved from the process analysis above, where the four ILs presented almost the same CO<sub>2</sub> recovery using equilibrium-based

simulations. In contrast, the CO<sub>2</sub> diffusion coefficients ( $D$ ) for each IL are remarkably different (Table 2), following the order EmimTCM > BmimTCM > BmimDCN > BmimOcSO<sub>4</sub>, and confirming the different absorption kinetic behavior revealed by process simulations (Figure 1). As can be seen, BmimOcSO<sub>4</sub> presents a particularly low CO<sub>2</sub> diffusion coefficient ( $D=1.8 \cdot 10^{-10} \text{ m}^2 \cdot \text{s}^{-1}$  at 301 K and 1 bar) compared to the other ILs ( $D = 8\text{-}9 \cdot 10^{-10} \text{ m}^2 \cdot \text{s}^{-1}$  at 301 K and 1 bar). For the long saturation times, we made the decision of only studying this IL at 301.5 K. Thus, the sequence of  $D$  values in Table 2 follows the same trend as the IL viscosity values (Table 1). Current experimental results are in agreement with the conclusions extracted in the previous section from process simulation, indicating that the efficiency of CO<sub>2</sub> capture by physical absorption can be severely limited in the case of ILs showing unfavorable transport properties, basically viscosity, even though they have a high CO<sub>2</sub> absorption capacity at equilibrium.

Table 1: Physical properties of selected ILs at 298.15 K

ILs	MW (g·mol <sup>-1</sup> )	$\rho$ (g·cm <sup>-3</sup> )	$\mu$ (cP)
EmimTCM	201.23	1.08 <sup>[34]</sup>	14.6 <sup>[35]</sup>
BmimTCM	229.28	1.05 <sup>[34]</sup>	28.5 <sup>[36]</sup>
BmimDCN	205.26	1.06 <sup>[35]</sup>	31.1 <sup>[36]</sup>
BmimOcSO <sub>4</sub>	348.50	1.06 <sup>[37]</sup>	669.4 <sup>[38]</sup>

Table 2: Experimental solubility and diffusion coefficients of selected ILs at different temperatures and pressures

$T$ (K)	ILs	Solubility			$z_{\text{CO}_2}$			$D$ ( $\cdot 10^{-11}$ )		
		(mg·g <sup>-1</sup> )			(mol·mol <sup>-1</sup> )			(m <sup>2</sup> ·s <sup>-1</sup> )		
		1 bar	3 bar	6 bar	1 bar	3 bar	6 bar	1 bar	3 bar	6 bar

	EmimTCM	3.8	11.1	22.2	0.017	0.048	0.092	90	125	150
301.5	BmimTCM	3.7	10.5	21.4	0.019	0.052	0.100	85	110	130
	BmimDCN	3.1	8.9	18.0	0.014	0.040	0.077	80	100	110
	BmimOcSO <sub>4</sub>	3.1	8.1	15.1	0.007	0.032	0.059	18	20	26
	EmimTCM	3.1	7.9	16.0	0.014	0.035	0.068	130	170	200
316.5	BmimTCM	2.9	7.9	16.0	0.015	0.040	0.077	120	150	170
	BmimDCN	2.4	6.7	13.5	0.011	0.030	0.059	110	140	155
	EmimTCM	2.3	6.1	11.5	0.010	0.027	0.050	160	205	250
331.5	BmimTCM	2.3	6.1	12.3	0.012	0.031	0.060	150	190	220
	BmimDCN	1.9	5.2	10.4	0.009	0.024	0.046	145	175	180

Uncertainties:  $u(P) = 0.01$  bar;  $u(solubility) = 0.01$  mg·g<sup>-1</sup>;  $u(z) = 0.0001$  mol·mol<sup>-1</sup>  $u(D)$

$= 25$  m<sup>2</sup>·s<sup>-1</sup>;  $u(T) = 0.1$  K

### ENIL preparation and characterization

In order to evaluate the role of IL encapsulation on the CO<sub>2</sub> capture by physical absorption with ILs, four ENILs were prepared and characterized using the ILs selected in the previous sections. Table 3 summarizes the characterization results of carbon capsules (C<sub>cap</sub>) and ENILs by means of elemental analysis and 77 K N<sub>2</sub> adsorption/desorption isotherms. As can be seen, the synthesized C<sub>cap</sub> presents a high BET surface area (1304 m<sup>2</sup>·g<sup>-1</sup>) and 93 % C content. Some amount of silica template may be remaining in the C<sub>cap</sub>, but not affecting the porous texture, morphology and functional properties. SEM and TEM images of C<sub>cap</sub> in Figure show a homogenous material composed of spheres with an external diameter around 750 nm and a shell thickness around 100 nm. Once the IL is incorporated, the accessible porosity of the C<sub>cap</sub> is filled by the IL, as can be observed from the low values of BET surface area (5 m<sup>2</sup>·g<sup>-1</sup>, accuracy of the equipment). As a result



of it, the carbonaceous surface in direct contact with the gas phase is almost negligible and the uptake of CO<sub>2</sub> can be attributed essentially to absorption. In addition, the IL fills the hollow carbon spheres. Thus, the IL content of all prepared ENILs, calculated by elemental analysis following the nitrogen content [21], is near 80 % (Table 3).

Table 3: ENIL and C<sub>cap</sub> characterization

		C <sub>cap</sub>	EmimTCM	BmimTCM	BmimDCN	BmimOcSO <sub>4</sub>
<b>A<sub>BET</sub> (m<sup>2</sup>·g<sup>-1</sup>)</b>		1304	< 5	< 5	< 5	< 5
<b>EA (% , w)</b>	<b>C</b>	93.0	60.8	67.8	62.5	62.1
	<b>H</b>	1.1	4.9	5.6	6.4	7.5
	<b>N</b>	0.1	27.8	24.9	27.3	6.3
<b>IL content (% , w)</b>		-	79.7	81.5	80.0	77.7

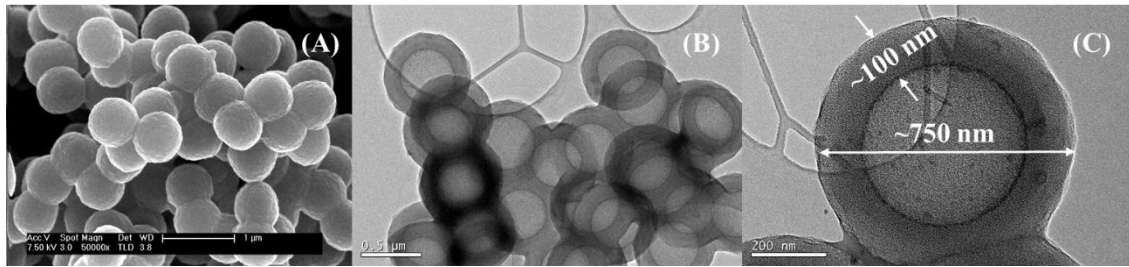


Figure 3: (A) SEM and TEM images (B, C) of C<sub>cap</sub> used as support for ENIL preparation.

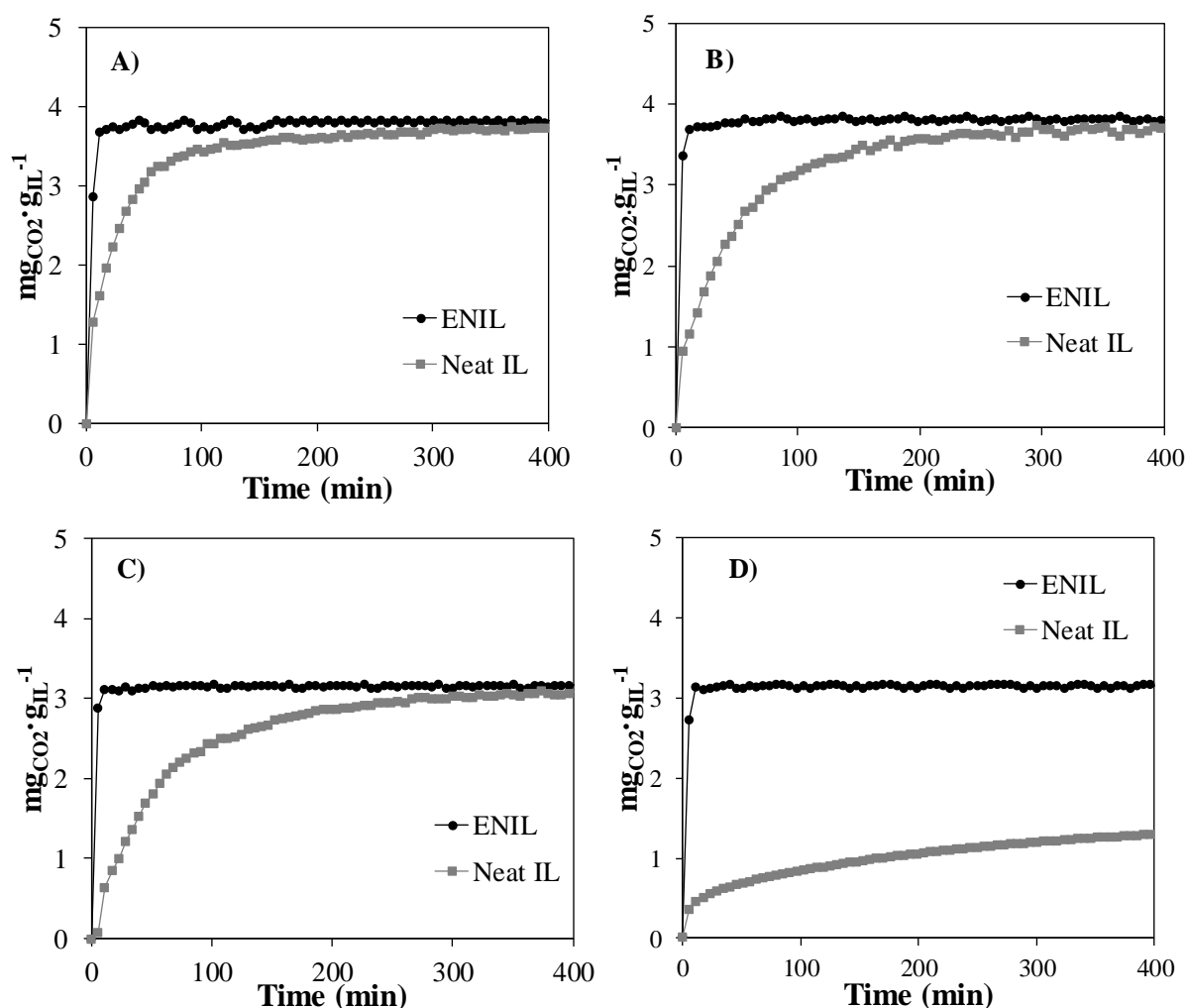


Figure 4: Kinetic curves of CO<sub>2</sub> uptake in ENIL and neat IL at 301.5 K and pCO<sub>2</sub> = 1 bar for A) EmimTCM, B) BmimTCM, C) BmimDCN and D) BmimOcSO<sub>4</sub>

### CO<sub>2</sub> sorption by ENIL materials

Figure 4 compares the kinetic curves of CO<sub>2</sub> uptake by ILs and ENIL materials obtained by gravimetric analysis at 301.5 K and 1 bar of CO<sub>2</sub> partial pressure. As can be seen, the uptake of CO<sub>2</sub> by neat ILs is much slower than for ENILS, and the neat ILs selected show very different saturation times, being EmimTCM the fastest (ca 300 min) and BmimOcSO<sub>4</sub> the slowest (> 600 min). The different behavior of the ILs selected is in agreement with the results from *Rate-based* process simulations and the experimental CO<sub>2</sub> diffusion values in ILs discussed above. Noticeably, the saturation time is greatly

reduced and nearly the same ( $\sim 10$  min) for all prepared ENILs, regardless of the IL used. These results indicate that the  $\text{CO}_2$  uptake rate is governed by the high contact area conferred to the IL by the morphology and small size of  $C_{\text{Cap}}$ , rather than by the mass transfer kinetics in the IL solvent. In good agreement with previous studies <sup>[15, 18-19]</sup>, the encapsulation of the ILs into the hollow microcapsules maintain the  $\text{CO}_2$  solubility in the IL (almost  $3 \text{ mg} \cdot \text{g}^{-1}$  in all cases) but drastically boosts the kinetics of the sorption process. Figure 5 presents the breakthrough curves of  $\text{CO}_2$  capture tests in fixed bed using ENIL as sorbents at three temperatures (303, 318 and 333 K) and 0.1 bar of  $\text{CO}_2$  partial pressure. Table 4 collects the characteristic thermodynamic and kinetic parameters obtained from the breakthrough curves. It should be remarked that the  $\text{CO}_2$  sorption capacities calculated for ENILs from the breakthrough curves nearly match the capacity values of neat ILs from the  $\text{CO}_2$  absorption isotherms obtained by gravimetry at different temperatures (see Figure 6A). Regarding kinetic aspects, Yoon and Nelson model can be considered to describe adequately the breakthrough curve slopes ( $R^2 > 0.98$ ). The estimated kinetic constants ( $k$  parameter in Table 4) fall within a narrow range, between 6 and  $10 \text{ min}^{-1}$ , for all the ILs and temperatures tested, in contrast with the variability of  $D_{\text{CO}_2}$  values from the absorption tests summarized in Table 2, where changes by a factor of 160 depending on the IL and temperature can be observed. The height of the mass transfer zone ( $H_{\text{MTZ}}$  in Table 4) is an additional parameter of interest to evaluate the performance of  $\text{CO}_2$  capture by ENILs. The breakthrough curves depicted in Figure 6 show a remarkable steep-shape for all the ENILs. Therefore,  $H_{\text{MTZ}}$  values are in a narrow range from 4 to 6 cm, slightly higher than those obtained with ENILs prepared with ILs that provide  $\text{CO}_2$  capture by chemical absorption <sup>[19]</sup> and in the order of  $H_{\text{MTZ}}$  values obtained in  $\text{CO}_2$  fixed bed capture using solid sorbents <sup>[39]</sup>. Consequently, using ENILs prepared with IL physical absorbent provides high bed utilization ( $f > 88\%$  for all ILs and temperatures)

(Table 4). These results reveal fast and favorable CO<sub>2</sub> physical sorption into ENILs in fixed-bed operation, ascribable to the large contact area and the small particle size, thus minimizing and overcoming the influence of mass transfer rate.

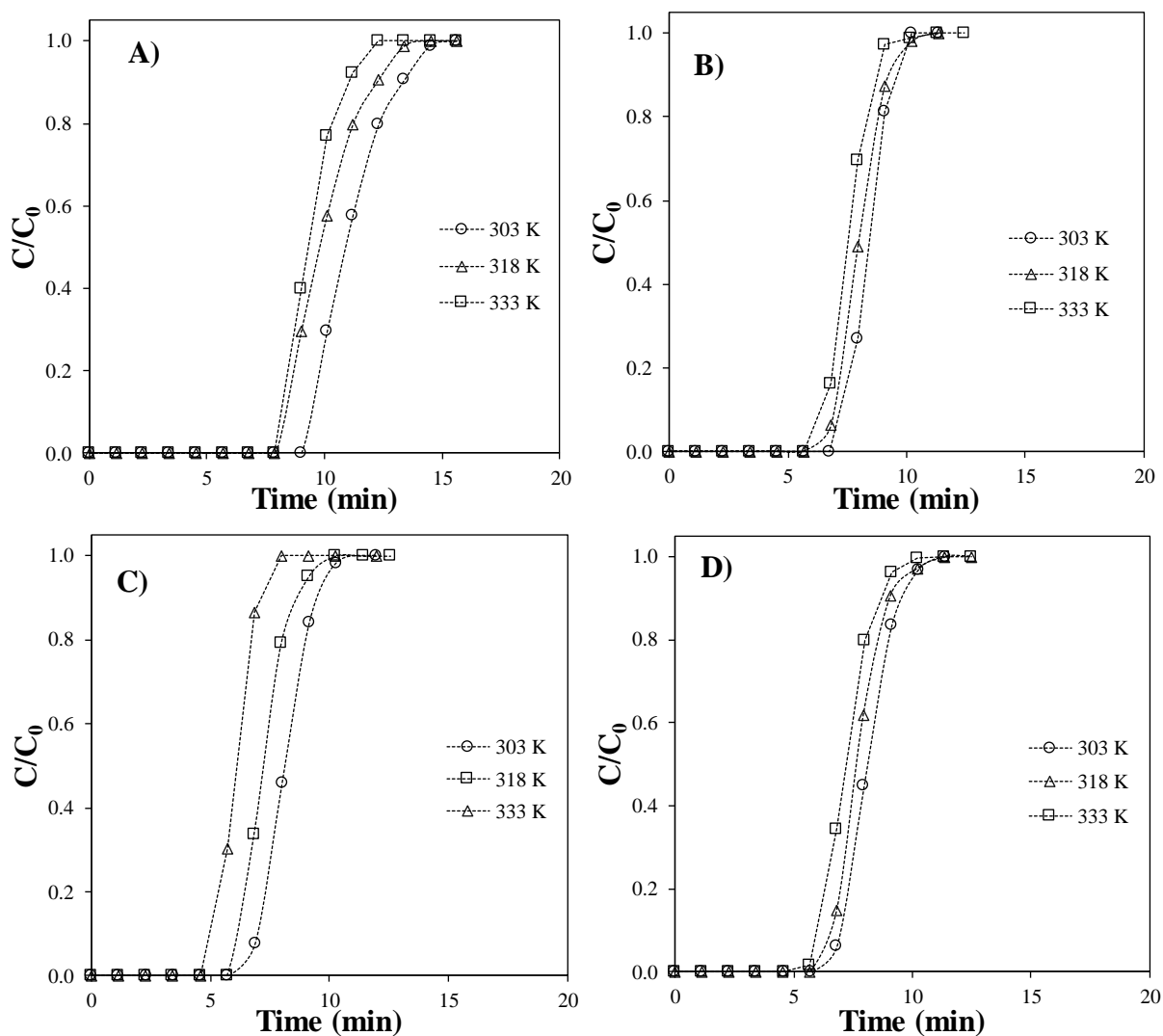


Figure 5: Breakthrough curves at different temperatures and 0.1 bar CO<sub>2</sub> partial pressure for ENILs prepared with A) EmimTCM, B) BmimTCM, C) BmimDCN and D) BmimOcSO<sub>4</sub>

Table 4: Operating conditions and results of the fixed bed CO<sub>2</sub> sorption experiments with the ENILs tested

ENIL	Fixed		$T$ (K)	$q_e$ (mg·g <sub>L</sub> <sup>-1</sup> )	$k$ (min <sup>-1</sup> )	$R^2$	$H_{MTZ}$ (cm)	$f$
	bed	mass (g)						
EmimTCM	3.36		303.1	0.43	8.5	0.996	4.5	0.85
			318.1	0.32	9.2	0.998	4.9	0.84
			333.1	0.26	9.9	0.996	5.9	0.80
BmimTCM	3.58		303.1	0.42	8.1	0.988	4.1	0.86
			318.1	0.31	9.0	0.994	4.8	0.84
			333.1	0.25	9.8	0.990	5.2	0.83
BmimDCN	4.15		303.1	0.33	7.6	0.998	4.8	0.84
			318.1	0.27	8.7	0.996	5.7	0.81
			333.1	0.20	9.5	0.996	6.1	0.80
BmimOcSO <sub>4</sub>	4.36		303.1	0.22	6.1	0.994	5.1	0.83
			318.1	0.19	7.5	0.984	5.9	0.81
			333.1	0.17	8.8	0.980	5.9	0.80

Uncertainties:  $u(\text{bed mass}) = 0.01$  g;  $u(T) = 0.1$  K;  $u(q_e) = 0.05$  mg·g<sup>-1</sup>;  $u(k) = 0.1$  min<sup>-1</sup>;  $u(H_{MTZ}) = 0.1$  cm;  $u(f) = 0.01$ .

The experimental values of the representative thermodynamic and kinetic parameters collected in Table 4 can be used to perform a process analysis similar to the one shown in Figure 1. Thus, simulations of fixed bed operation with the four ENILs tested at fixed operating conditions were conducted to estimate CO<sub>2</sub> recovery, using an ideal equilibrium model where mass transfer limitations are not considered (equivalent to *Equilibrium*

mode) and the Yoon and Nelson model (equivalent to *Rate-based* mode). For this purpose, the breakthrough curves for the four ENILs were simulated considering a bed with 1 kg of sorbent and an inlet flow of 100 Nml/min of a stream with a CO<sub>2</sub> concentration of 10% at 303 K, maintaining constant the space velocity in the simulation of scaled-up bed. For the equilibrium recovery, a kinetic constant of infinite value is considered, which results in a breakthrough curve with infinite slope value placed at  $t_{0.5}$ . The results of this analysis are collected in Figure 6B.

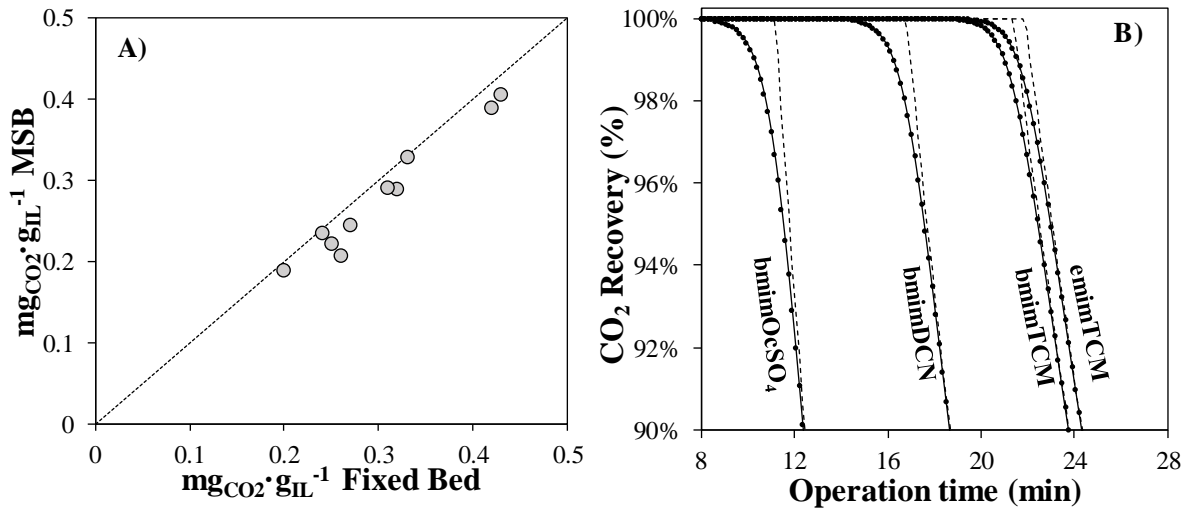


Figure 6: **A)** CO<sub>2</sub> solubility in ENIL materials (IL basis) measured in MSB and fixed bed reactor at  $p_{\text{CO}_2} = 0.1$  bar and three different temperatures (303, 318 and 333 K). **B)** CO<sub>2</sub> recovery in fixed bed operation over time with ENILs, calculated using the Yoon and Nelson model (symbols) and the ideal equilibrium model (dash-line).

The differences in CO<sub>2</sub> recoveries obtained with the ideal equilibrium model and Yoon and Nelson model simulations in a fixed bed with the different ENILs are in the range of 2 - 4 %. This implies that in a conventional fixed bed operation the ENIL sorbent can be almost fully saturated and that the separation efficiency, i.e. the amount of CO<sub>2</sub> captured

per mass of IL used, can be increased by using ILs where CO<sub>2</sub> is more soluble, even if they do not have good mass transfer-related properties. Figure 6B can be analyzed in terms of CO<sub>2</sub> recovery at a fixed breakthrough time; for instance, the time at which the CO<sub>2</sub> concentration at the outlet reaches 10% of the inlet value when using EmimTCM-ENIL. At such time, CO<sub>2</sub> recoveries (EmimTCM: 99 %, BmimTCM: 99 %, bmimDCN: 81 %, bmimOcSO<sub>4</sub>: 54 %) are clearly related to experimental absorption capacity (Table 2) but not to the diffusion coefficient of CO<sub>2</sub> in neat ILs (Table 2). In sum, these results indicate that the encapsulation of the ILs in ENILs makes possible to use them in fixed bed operation overcoming the mass transfer limitations of the CO<sub>2</sub> capture process by physical absorption, being the solubility of CO<sub>2</sub> in the IL the main parameter to be considered for the design.

## Conclusions

Encapsulated ionic liquids (ENIL materials) are proposed for overcoming the mass transfer limitations that neat ILs present in the physical absorption of CO<sub>2</sub>. *RADFRAC* absorption columns on *Equilibrium* and *Rate-based* modes of Aspen Plus software were simulated for 44 ILs from ILUAM database showing a wide range of recoveries in both modes. EmimTCM, BmimTCM, BmimDCN, and BmimOcSO<sub>4</sub> were selected for the experimental determination of CO<sub>2</sub> solubilities and diffusivities by gravimetric analysis. The results are in agreement with those from process simulation, yielding almost the same CO<sub>2</sub> solubility values (3 mg·g<sup>-1</sup> at 301 K) for the four ILs tested and markedly different CO<sub>2</sub> diffusivity values. In order to solve these mass transfer limitations, ENILs were prepared with the selected ILs and tested in an MSB equipment, showing that the solubility of the IL loaded is maintained while the mass transfer rate is enhanced and the

saturation time is reduced by two orders of magnitude. Finally, the ENILs were tested in CO<sub>2</sub> capture using fixed beds, showing no significant differences in absorption rate and a bed utilization determined mainly by the solubility of CO<sub>2</sub> in the ILs. Therefore, these results demonstrate the fast CO<sub>2</sub> mass transfer rates in ENILs -related to the high contact area provided- allows overcoming the mass transfer limitations that typically control the rate of physical absorption of CO<sub>2</sub> in neat ILs.

## Acknowledgments

The authors are grateful to Comunidad de Madrid (project *S2013-MAE-2800*) and Ministerio de Economía y Competitividad of Spain (project *CTQ2017-89441-R*) for financial support and Centro de Computación Científica de la Universidad Autónoma de Madrid for computational facilities. Marcos Larriba also thanks MINECO for awarding him a Juan de la Cierva-Formación Contract (Reference FJCI-2015-25343).

## References

- [1] a) M. K. Mondal, H. K. Balsora and P. Varshney, *Energy* **2012**, *46*, 431-441; b) M. Wang, A. Lawal, P. Stephenson, J. Sidders and C. Ramshaw, *Chemical Engineering Research and Design* **2011**, *89*, 1609-1624.
- [2] J. D. Figueroa, T. Fout, S. Plasynski, H. McIlvried and R. D. Srivastava, *International Journal of Greenhouse Gas Control* **2008**, *2*, 9-20.
- [3] C.-H. Yu, *Aerosol and Air Quality Research* **2012**.
- [4] P. D. Vaidya and V. V. Mahajani, *Industrial & Engineering Chemistry Research* **2005**, *44*, 1868-1873.
- [5] C. J. Chang, C. Y. Day, C. M. Ko and K. L. Chiu, *Fluid Phase Equilibria* **1997**, *131*, 243-258.
- [6] A.-L. Revelli, F. Mutelet and J.-N. Jaubert, *Journal of Physical Chemistry B* **2010**, *114*, 12908-12913.
- [7] a) G. Ferrara, A. Lanzini, P. Leone, M. T. Ho and D. E. Wiley, *Energy* **2017**, *130*, 113-128; b) G. T. Rochelle, *Science* **2009**, *325*, 1652-1654.
- [8] J. Kothandaraman, A. Goeppert, M. Czaun, G. A. Olah and G. K. S. Prakash, *Green Chemistry* **2016**, *18*, 5831-5838.
- [9] S. Tang, G. A. Baker and H. Zhao, *Chem Soc Rev* **2012**, *41*, 4030-4066.



- [10] a) K. Anderson, M. P. Atkins, J. Estager, Y. Kuah, S. Ng, A. A. Oliferenko, N. V. Plechkova, A. V. Puga, K. R. Seddon and D. F. Wassell, *Green Chemistry* **2015**, *17*, 4340-4354; b) C. Wang, H. Luo, X. Luo, H. Li and S. Dai, *Green Chemistry* **2010**, *12*, 2019-2023; c) E. I. Izgorodina, J. L. Hodgson, D. C. Weis, S. J. Pas and D. R. MacFarlane, *The Journal of Physical Chemistry B* **2015**, *119*, 11748-11759; d) S. Sarmad, J. P. Mikkola and X. Ji, *ChemSusChem* **2017**, *10*, 324-352; e) S. Zeng, X. Zhang, L. Bai, X. Zhang, H. Wang, J. Wang, D. Bao, M. Li, X. Liu and S. Zhang, *Chemical Reviews* **2017**, *117*, 9625-9673.
- [11] M. Bui, C. S. Adjiman, A. Bardow, E. J. Anthony, A. Boston, S. Brown, P. S. Fennell, S. Fuss, A. Galindo, L. A. Hackett, J. P. Hallett, H. J. Herzog, G. Jackson, J. Kemper, S. Krevor, G. C. Maitland, M. Matuszewski, I. S. Metcalfe, C. Petit, G. Puxty, J. Reimer, D. M. Reiner, E. S. Rubin, S. A. Scott, N. Shah, B. Smit, J. P. M. Trusler, P. Webley, J. Wilcox and N. Mac Dowell, *Energy & Environmental Science* **2018**.
- [12] a) C. Wu, T. P. Senftle and W. F. Schneider, *Phys Chem Chem Phys* **2012**, *14*, 13163-13170; b) J. Huang and T. Ruether, *Australian Journal of Chemistry* **2009**, *62*, 298-308.
- [13] J. de Riva, J. Suarez-Reyes, D. Moreno, I. Díaz, V. Ferro and J. Palomar, *International Journal of Greenhouse Gas Control* **2017**, *61*, 61-70.
- [14] J. E. Brennecke and B. E. Gurkan, *Journal of Physical Chemistry Letters* **2010**, *1*, 3459-3464.
- [15] J. Palomar, J. Lemus, N. Alonso-Morales, J. Bedia, M. A. Gilarranz and J. J. Rodriguez, *Chem Commun (Camb)* **2012**, *48*, 10046-10048.
- [16] N. Alonso-Morales, M. A. Gilarranz, J. Palomar, J. Lemus, F. Heras and J. J. Rodriguez, *Carbon* **2013**, *59*, 430-438.
- [17] a) J. Lemus, J. Palomar, M. A. Gilarranz and J. J. Rodriguez, *Adsorption* **2011**, *17*, 561-571; b) J. Lemus, C. Neves, C. F. C. Marques, M. G. Freire, J. A. P. Coutinho and J. Palomar, *Environmental Science-Processes & Impacts* **2013**, *15*, 1752-1759.
- [18] J. Lemus, J. Bedia, C. Moya, N. Alonso-Morales, M. A. Gilarranz, J. Palomar and J. J. Rodriguez, *Rsc Advances* **2016**, *6*, 61650-61660.
- [19] C. Moya, N. Alonso-Morales, M. A. Gilarranz, J. J. Rodriguez and J. Palomar, *ChemPhysChem* **2016**, *17*, 3891-3899.
- [20] J. Lemus, F. A. Da Silva F, J. Palomar, P. J. Carvalho and J. A. P. Coutinho, *Separation and Purification Technology* **2017**.
- [21] K. Dong, X. Liu, H. Dong, X. Zhang and S. Zhang, *Chemical Reviews* **2017**, *117*, 6636-6695.
- [22] V. R. Ferro, C. Moya, D. Moreno, R. Santiago, J. de Riva, G. Pedrosa, M. Larriba, I. Diaz and J. Palomar, *Industrial & Engineering Chemistry Research* **2018**, *57*, 980-989.
- [23] V. R. Ferro, E. Ruiz, J. de Riva and J. Palomar, *Separation and Purification Technology* **2012**, *97*, 195-204.
- [24] J. Bedia, E. Ruiz, J. de Riva, V. R. Ferro, J. Palomar and J. J. Rodriguez, *AIChE Journal* **2013**, *59*, 1648-1656.
- [25] R. Santiago, J. Bedia, D. Moreno, C. Moya, J. de Riva, M. Larriba and J. Palomar, *Separation and Purification Technology*.
- [26] a) J. de Riva, V. R. Ferro, D. Moreno, I. Diaz and J. Palomar, *Fuel Processing Technology* **2016**, *146*, 29-38; b) M. Larriba, J. de Riva, P. Navarro, D. Moreno, N. Delgado-Mellado, J. Garcia, V. R. Ferro, F. Rodriguez and J. Palomar, *Separation and Purification Technology* **2018**, *190*, 211-227.
- [27] I. Diaz, J. Palomar, M. Rodriguez, J. de Riva, V. Ferro and E. J. Gonzalez, *Chemical Engineering Research & Design* **2016**, *115*, 382-393.
- [28] a) E. Ruiz, V. R. Ferro, J. de Riva, D. Moreno and J. Palomar, *Applied Energy* **2014**, *123*, 281-291; b) D. Moreno, V. R. Ferro, J. de Riva, R. Santiago, C. Moya, M. Larriba and J. Palomar, *Applied Energy* **2018**, *213*, 179-194.
- [29] G. Büchel, K. K. Unger, A. Matsumoto and K. Tsutsumi, *Advanced Materials* **1998**, *10*, 1036-1038.
- [30] C. Moya, J. Palomar, M. Gonzalez-Miquel, J. Bedia and F. Rodriguez, *Industrial and Engineering Chemistry Research* **2014**, *53*, 13782-13789.

- [31] M. B. Shiflett and A. Yokozeki, *Industrial & Engineering Chemistry Research* **2005**, *44*, 4453-4464.
- [32] Y. H. Yoon and J. H. Nelson, *American Industrial Hygiene Association Journal* **1992**, *53*, 303-316.
- [33] a) J. Lemus, M. Martin-Martinez, J. Palomar, L. Gomez-Sainero, M. A. Gilarranz and J. J. Rodriguez, *Chemical Engineering Journal* **2012**, *211-212*, 246-254; b) Y. H. Yoon and J. H. Nelson, *American Industrial Hygiene Association Journal* **1984**, *45*, 517-524.
- [34] M. Součková, J. Klomfar and J. Pátek, *Fluid Phase Equilibria* **2015**, *406*, 181-193.
- [35] C. M. S. S. Neves, K. A. Kurnia, J. A. P. Coutinho, I. M. Marrucho, J. N. C. Lopes, M. G. Freire and L. P. N. Rebelo, *The Journal of Physical Chemistry B* **2013**, *117*, 10271-10283.
- [36] P. J. Carvalho, T. Regueira, L. M. N. B. F. Santos, J. Fernandez and J. A. P. Coutinho, *Journal of Chemical & Engineering Data* **2010**, *55*, 645-652.
- [37] M. J. Davila, S. Aparicio, R. Alcalde, B. Garcia and J. M. Leal, *Green Chemistry* **2007**, *9*, 221-232.
- [38] J. Jacquemin, P. Husson, V. Majer, A. A. H. Padua and M. F. C. Gomes, *Green Chemistry* **2008**, *10*, 944-950.
- [39] A. M. Mastral, T. García, R. Murillo, M. S. Callén, J. M. López and M. V. Navarro, *Industrial & Engineering Chemistry Research* **2003**, *42*, 5280-5286.